Polymer Journal (2012) 44, 658–664

www.nature.com/pj

ORIGINAL ARTICLE

Rapid and reversible morphology control in thin films of poly(ethylene oxide)-block-POSS-containing poly(methacrylate)

Raita Goseki, Tomoyasu Hirai, Yoshihito Ishida, Masa-aki Kakimoto and Teruaki Hayakawa

Here we report rapid control of the morphology of a polyhedral oligomeric silsesquioxane (POSS)-containing block copolymer (PEO_{143}-*b*-$PMAPOSS_{12}$), which is composed of poly(ethylene oxide) (PEO) and POSS-containing poly(methacrylate), (PMAPOSS), between ordered arrays of dots and lines for several tens of seconds by a combination of thermal annealing and solvent annealing. The PEO_{143}-*b*-$PMAPOSS_{12}$ was synthesized by atom transfer radical polymerization of POSS methacrylate by using a macroinitiator of PEO. An ordered array of dots was obtained by thermal annealing for the as-spun cast thin film at 90 °C for 60 s. The resultant ordered dots were quickly converted to lines by solvent annealing with chloroform vapor at room temperature for 120 s. The lines were converted back to dots by thermal annealing under the same conditions (90 °C, 60 s) without any changes to the initial diameter, *d*-spacing or thickness. We also demonstrated the simple and rapid formation of a hexagonally packed array of dots by spin casting onto a trench-patterned silicon wafer under chloroform vapor. Under thermal and solvent annealing conditions, reversibility and a high degree of ordering in the phase morphology of PEO_{143}-*b*-$PMAPOSS_{12}$ are distinctive properties that can be attributed to highly mobile polymer chains.
Polymer Journal (2012) **44,** 658–664; doi:10.1038/pj.2012.67; published online 18 April 2012

Keywords: annealing; block copolymer; polyethylene oxide (PEO); polyhedral oligomeric silsesquioxane (POSS); self-assembly; thin film

INTRODUCTION

The self-assembly of thin films from block copolymers (BCPs) has attracted a considerable research interest because of the potential applications to plasmonic waveguides, magnetic logic gates, magnetic data storage and microelectronic devices.[1–7] Block copolymer lithography (BCPL) is a promising next generation lithographic technique that could be used for high-throughput and large-area nanolithography; BCPL utilizes the self-assembled nanostructures that form by microphase separation of BCP in thin films.[8–12] The vast majority of research on self-assembling polymers for BCPL has been devoted to polystyrene-*block*-poly(methyl methacrylate) because the PMMA block can be selectively removed by ultraviolet or oxygen plasma exposure.[13–15] Despite significant progress, controlling the orientation and long-range ordering of the microphase-separated nanodomains in the thin films remains a formidable technological challenge in terms of feature sizes. It is difficult to form features with a full pitch size <20 nm with most BCPs because of their small Flory–Huggins interaction parameter. Silicon-containing BCPs, such as poly(styrene-*block*-dimethylsiloxane) (PS-*b*-PDMS),[16–18] PS-*block*-poly(ferrocenylsilane)[19–21] and PMMA-*block*-polyhedral oligomeric silsesquioxane (POSS)-containing poly(methacrylate), (PMMA-*b*-PMAPOSS), are considered to be more strongly segregating BCPs and have been well characterized in studies looking to overcome the limit of feature sizes. We have reported the development and study of a series of silicon-containing PMAPOSS-based BCPs.[22–26] These polymers can self assemble with much smaller periodic features ($\geqslant 10$ nm) because they exhibit strongly segregating microphases. A high etch contrast can also be achieved between the polymer domains. These findings are consistent with studies of the self-assembled nanostructures in silicon-containing PMAPOSS and other hydrocarbon polymers such as PS and PMMA, using oxygen plasma for dry etching.[23] This can lead to reliable high-resolution patterns in BCPL. Recently, we showed the successful formation of long-range ordered arrays of dots with densities of ~ 4 tera dots per square inch for PMMA-*b*-PMAPOSSs through directed self-assembly, with density multiplication of the chemically patterned template.[27]

The control of phase morphology with a long-range order in BCP thin films has recently attracted an increasing interest for the patterning of two self-assembled phase morphologies within a single block copolymer film onto a specific area.[28,29] Both thermal annealing and solvent annealing are well known and appealing methods for controlling the phase morphology by reassembly of the polymer

Department of Organic and Polymeric Materials, Tokyo Institute of Technology, Meguro-ku, Tokyo, Japan
Correspondence: Professor T Hayakawa, Department of Organic and Polymeric Materials, Tokyo Institute of Technology, 2-12-1-S8-36 O-okayama, Meguro-ku, Tokyo 152-8552, Japan.
E-mail: hayakawa.t.ac@m.titech.ac.jp
Received 1 February 2012; revised 10 March 2012; accepted 12 March 2012; published online 18 April 2012

chains.[30–33] Reversible tuning of the morphologies is also possible by controlling the annealing conditions. In our previous study, we attempted to control the phase morphology and long-range ordering of the microphase-separated nanostructures of a series of POSS-containing BCPs.[22–27] The solvent annealing strongly affected the growth and reformation of the assemblies in the as-cast thin films of PS-*b*-PMAPOSS and PMMA-*b*-PMAPOSS, resulting in long-range ordered arrays of dots and lines. However, a long duration of annealing, from several minutes to hours, was necessary. A simple and brief annealing BCPL process is essential for high-throughput manufacturing. Conversely, in the thermal annealing process, no effective reassembly was observed in these BCPs. This response might be because of the insufficient mobility of the polymer chains for diffusing and undergoing microphase separation to form the self-assembled structure in thermodynamic equilibrium. Achieving this customizable control of phase morphology in lithographically patterned BCP materials, especially for silicon-containing BCPs in BCPL, could provide many opportunities to extend a variety of nanopatterned templates. Challenges remain in controlling the self-assembly of polymers at short annealing durations by optimizing the annealing conditions. To overcome these issues, it is important to also improve the molecular structure of BCPs.

Here we demonstrate the rapid and reversible control of the morphology of POSS-containing BCP thin films by thermal annealing and solvent annealing. This control is enabled by the distinctive properties of PEO-*b*-PMAPOSS (PEO-*b*-PMAPOSS).[34,35] Each PS and PMMA, as a hydrocarbon polymer segment in POSS-containing BCPs, exists in the amorphous state over a wide range of temperatures during thermal annealing. In contrast, crystalline PEO usually melts at relatively low temperatures $<60\,^{\circ}C$. Therefore, by introducing PEO into the POSS-containing BCP as the hydrocarbon segment instead of PS and PMMA, the PEO at an isotropic state possesses highly mobile chains, which would contribute to sufficient diffusing and reassembly of the POSS-containing BCP. In this study, we show that thermal annealing for short durations (60 s) provides highly ordered spherical domains of poly(ethylene oxide; PEO in as-cast thin films. We also describe the reversible tuning of the phase morphologies in the thin films. Furthermore, we also demonstrate the easy and rapid formation of hexagonally packed dot arrays in the thin films prepared by spin casting onto a trench-patterned silicon wafer under chloroform vapor, without additional annealing.

EXPERIMENTAL PROCEDURE

Materials

Bromo-terminated PEO_{143} (PEO macroinitiator: $M_n = 6300$) was purchased from SOWA SCIENCE CO. (Ibaraki, Japan) and used as received. POSS methacrylate with isobutyl substituents (MAPOSS) was purchased from Hybrid Plastics (Hattiesburg, MS, USA) and was recrystallized from methanol before use. *N,N,N′,N′,N″*-pentamethyldiethylenetriamine (PMDETA; 99%) and cupper chloride (I; $Cu^{I}Cl$; 99%) were purchased from Sigma-Aldrich Japan Co. (Tokyo, Japan). PMDETA was distilled over calcium hydride under nitrogen. $Cu^{I}Cl$ was purified by washing with acetic acid. Toluene was distilled over sodium under nitrogen.

Synthesis of PEO-*b*-PMAPOSS

MAPOSS (1.0 g, 0.973 mmol), $Cu^{I}Cl$ (2.3 mg, 0.024 mmol), toluene (60 wt % relative to monomer) and PMDETA (1.0 ml, 4.78 mmol) were added to a 20-ml Schlenk flask with a magnetic stirrer bar. The mixture was degassed by three cycles of freeze-pump-thaw. Then, a PEO macroinitiator (0.288 g, 0.048 mmol (-Br)) was dissolved in toluene (0.5 ml) and added via a syringe after the copper complex was allowed to form. The Schlenk flask was then placed in an oil bath at 50 °C for 24 h. The polymer solution was filtered through neutral alumina and purified by column chromatography on silica, using chloroform and gradually increasing the amount of tetrahydrofuran to the ratio of 1:1 chloroform/tetrahydrofuran and then to a pure tetrahydrofuran. The solvent was removed, acetone was added to remove (by precipitation) the unreacted PEO macroinitiator, the solution was filtered and the obtained polymer was dried *in vacuo* at room temperature for 3 h. The polymer yield was 49%. ^{1}H nuclear magnetic resonance (NMR) (300 MHz, $CDCl_3$ δ): 3.82 (br, -O-CH_2), 3.6 (s, -(CH_2-CH_2-O-)-), 3.38 (s, PEO terminal CH_3-O-), 1.87–1.53 (m, isobutyl -C*H*, main chain-CH_2), 0.95–0.93 (br, isobutyl -C(CH_3)$_2$), 0.59 (br, -SiCH_2) p.p.m. ^{13}C NMR (75 MHz, $CDCl_3$, δ): 176.9, 67.2, 45.2, 26.0, 25.8, 25.7, 25.5, 24.0, 23.8, 22.5, 21.4 and 8.4 p.p.m. ^{29}Si NMR (MHz, $CDCl_3$, δ); −59.2 p.p.m. Infrared (KBr): $\nu = 2954$, 2871, 1732, 1446, 1366, 1332, 1232 and 1106 cm^{-1}.

Bulk morphology

The sample of PEO_{143}-*b*-$PMAPOSS_{12}$ for investigating the bulk morphology was prepared by drop-casting from chloroform solution onto a silicon wafer and subsequently annealing at 90 °C in vacuum for 1 h.

Thin film preparation

Thin films were prepared (without any environment control) by spin casting from a polymer solution in chloroform (0.8–2.0 wt%) onto silicon wafers containing its native oxide at 4000 r.p.m. for 60 s. The wafers were cleaned before spin casting. The substrates were cleaned using a piranha solution containing a mixture of H_2O_2 (30%)/H_2SO_4 (70%) (*v*/*v*) at 110 °C for 2 h, rinsed with distilled water and dried in a stream of nitrogen. Film thicknesses were altered by spin casting from the polymer solution of varying concentrations. The film thickness was measured using an ellipsometer or Filmetrics F20 (Filmetrics, Inc., Kanagawa, Japan). The film thickness was monitored *in situ* with a Filmetrics F20 in the reflectance mode, with a blank silicon slide as a reference. O_2-RIE experiments were performed by oxygen plasma etching, for a certain seconds at 50 W and 40 sccm oxygen.

Instruments

NMR spectra were taken on a JEOL JNM-AL 300 spectrometer (JEOL, Tokyo, Japan) operating at 300 MHz for ^{1}H, 75 MHz for ^{13}C and 59.4 MHz for ^{29}Si, respectively, using tetramethylsilane as the internal standard. Infrared spectra was recorded on a JASCO Fourier Transform IR-460 Plus spectrometer (JASCO, Tokyo, Japan). The glass transition temperature (T_g) and melting temperature (T_m) were measured with a Seiko SSC/6000 (DSC 6200, SII Nano Technology Inc., Chiba, Japan) under nitrogen (heating rate 10 °C min^{-1}, nitrogen flow rate 50 ml min^{-1}). Thermogravimetric analyses were performed with a Seiko SSC/6000 (TG/DTA 6200) under nitrogen (heating rate 10 °C min^{-1}, nitrogen flow rate 50 ml min^{-1}). Samples weighing ~5 mg were used for the thermogravimetric and differential scanning calorimetry measurements. Molecular weights and molecular weight distributions were estimated using a Shodex RI-71 (Showa Denko Co., Tokyo, Japan) and size exclusion chromatography on a Shodex GPC-101, using two consecutive linear polystyrene gel columns (Shodex KF-802 and Shodex KF-806M) at a flow rate of 1 ml min^{-1} at 40 °C. These measurements were performed according to polystyrene standards using tetrahydrofuran as the eluent and Shodex RI-71 as detectors. Small angle X ray scattering (SAXS) was performed using a Bruker NanoSTAR (Bruker AXS K.K., Kanagawa, Japan, 50 kV per 100 mA) with a 2D-PSPC detector (camera length 1055 nm). Wide angle X-ray diffraction was recorded on a flat imaging plate by using Cu Kα radiation generated by a Bruker NanoSTAR. Tapping mode atomic force microscopy measurements were performed on Seiko model SPA-400. Scanning electron microscopy (SEM) images of PEO_{143}-*b*-$PMAPOSS_{12}$ thin films were obtained using a Hitachi S-4800 SEM secondary electron microscope (Hitachi, Tokyo, Japan) with a field emission source at 1.0 kV.

RESULTS AND DISCUSSION

Synthesis and characterization of PEO-*b*-PMAPOSS

The desired POSS-containing BCP, PEO-*b*-PMAPOSS, was prepared by atom transfer radical polymerization of POSS methacrylate monomer at 50 °C for 24 h (Figure 1). The polymerization was

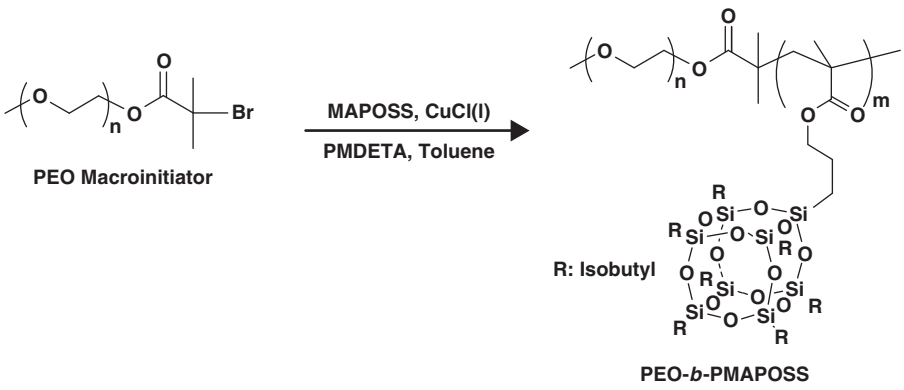

Figure 1 Synthesis scheme for PEO_{143}-*b*-$PMAPOSS_{12}$.

performed in the presence of a PEO macroinitiator ($M_n = 6300$ g mol^{-1}), Cu^ICl and PMDETA in anhydrous toluene as a solvent. The chemical structure and the composition of the resultant PEO-*b*-PMAPOSS were characterized by ^1H, ^{13}C, ^{29}Si NMR and Infrared spectroscopy. The ^1H NMR spectrum in *d*-chloroform is shown in Figure 2. The signals observed at 0.59 and 3.9 p.p.m. correspond to -SiCH_2 from the POSS cage and to the PEO ethylene segment (-CH_2-CH_2-O-), respectively. The number-average molecular weight (M_n) and the polydispersity index of PEO-*b*-PMAPOSS against linear PS standards were $M_n = 18\,600$ g mol^{-1} and polydispersity index 1.20. The composition of PEO_{143}-*b*-$PMAPOSS_{12}$ was estimated from the ^1H NMR spectrum by using the ratio of the integrated intensities of the signals for the ethylene protons in PEO and the methylene protons in POSS, and using the density of PEO (1.21 g cm^{-3}) and PMAPOSS (1.14 g cm^{-3}).[24] On the basis of these calculations, it was determined that the volume ratio of the polymer was 11% PEO and 89% PMAPOSS for each block. The thermal behavior of PEO_{143}-*b*-$PMAPOSS_{12}$ was examined by thermogravimetric and differential scanning calorimetry. We first confirmed that no significant weight loss was observed $<280\,^\circ$C by thermogravimetric analysis. To eliminate the effect of thermal history on sample transitions, the sample was heated to 180 °C and held for 1 min at this temperature before cooling to $-70\,^\circ$C at a rate of 10 °C min^{-1}. Differential scanning calorimetry data were obtained from the second run. As shown in Figure 3, two distinct transitions were observed at 50 °C and 82 °C in the heating cycle, which correspond to the T_m of PEO and the T_g of PMAPOSS,[36] respectively. The T_m of PEO in PEO_{143}-*b*-$PMAPOSS_{12}$ is observed at a lower temperature in comparison with the PEO macroinitiator ($T_m = 57\,^\circ$C). During the cooling cycle, the T_g of PMAPOSS and the T_m of PEO are shown at 42 °C and $-29\,^\circ$C, respectively.

To investigate the oxygen plasma etching resistance of PEO homopolymer to PMAPOSS and other hydrocarbon polymers like PS and PMMA, thin films were prepared from 3.0% (*w*/*w*) polymer solution in chloroform onto a silicon wafer. The thickness was measured by an ellipsometer after a given duration of exposure (0, 30, 60 and 120 s) to oxygen plasma. It can be observed from Figure 4 that the etch depth of PEO increases linearly with time at an etching rate of 32.0 nm s^{-1}. The etch amount of PMAPOSS corresponds to about 1/21 of PEO's etch amount. These results indicate that relatively highly etching contrast can be expected in the PEO-*b*-PMAPOSS lithographic patterns by oxygen plasma etching.

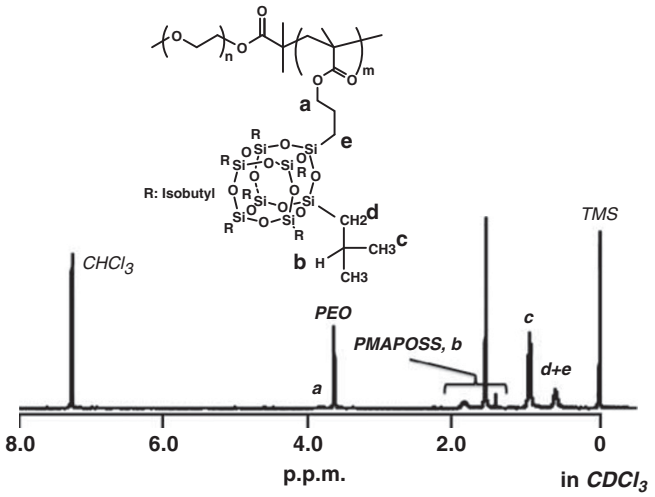

Figure 2 ^1H NMR spectrum of PEO_{143}-*b*-$PMAPOSS_{12}$ in $CDCl_3$.

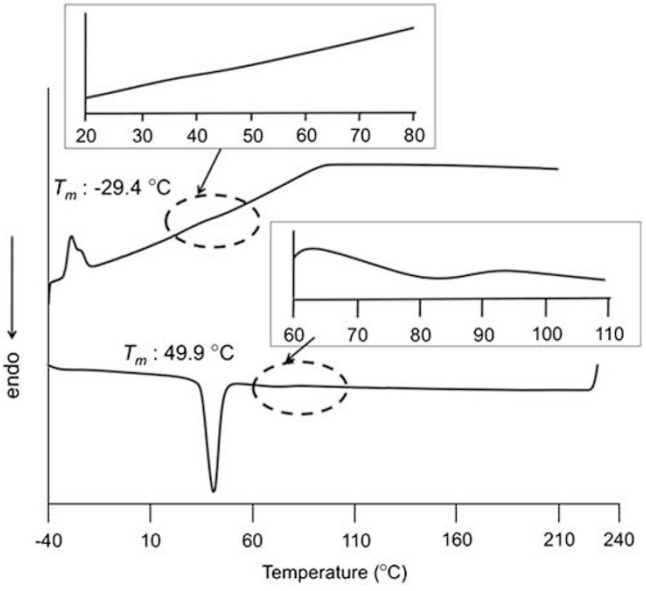

Figure 3 Differential scanning calorimetry curve of PEO_{143}-*b*-$PMAPOSS_{12}$.

Bulk morphology characterization

To characterize the bulk morphology of PEO_{143}-*b*-$PMAPOSS_{12}$, the sample was prepared by slow evaporation from the polymer solution in chloroform and then annealed at 90 °C for 1 h at a reduced pressure. The sample was evaluated by wide angle X-ray diffraction, SAXS, TEM and SEM. Figures 5a and b show wide angle X-ray

diffraction and SAXS results of PEO_{143}-*b*-$PMAPOSS_{12}$, respectively. The wide angle X-ray diffraction patterns show four broad diffraction peaks at a *d*-spacing of 1.01, 0.74, 0.43 and 0.38 nm, which corresponds to the POSS aggregation in the bulk.[37] The PEO macroinitiator also shows two diffraction peaks at a *d*-spacing of 0.43 and 0.38 nm. The diffraction patterns overlap in the profile and reveal the crystalline states of the PEO and PMAPOSS segments. Conversely, four peaks with scattering ratios of 1, $3^{1/2}$, $4^{1/2}$ and $7^{1/2}$ were observed in the SAXS profile. Because the TEM image for the same sample with SAXS was blurred, we attempted to investigate the microphase-separated nanostructure using SEM. The sample for SEM was prepared by drop-casting the polymer onto a silicon wafer and annealing it at 90 °C for 1 h. Figure 5c shows a typical film thickness with spherical microdomains, in which the spheres correspond to the PEO domains. The PMAPOSS blocks tend to discharge more secondary electrons than the PEO blocks because the PMAPOSS blocks contain Si atoms. Therefore, the darker domains in the SEM images correspond to the PEO. A typical scattering peak at $2^{1/2}$ for a body-centered-cubic lattice of self-assembled spherical microdomains is difficult to find in the profile owing to the low degree of order in the morphology. However, we conclude that the PEO domains are spherical in the thermally annealed PEO_{143}-*b*-$PMAPOSS_{12}$. The *d*-spacing of spherical domains is 15.7 nm, as calculated from the SAXS profile.

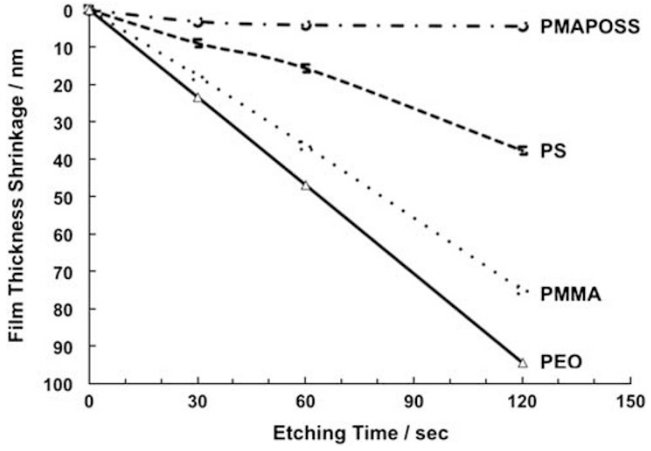

Figure 4 Graph of the etch amount for PEO, PS, PMMA and PMAPOSS homopolymers with increasing exposure to oxygen plasma.

Morphology control of microphase-separated nanostructures in thin films

We first focused our experiments on the control of phase morphologies in the PEO_{143}-*b*-$PMAPOSS_{12}$ thin films by thermal annealing and solvent annealing. Thin films were prepared by spin casting a solution containing 1 wt% of PEO_{143}-*b*-$PMAPOSS_{12}$ in chloroform onto silicon wafers. The thickness of the film was well controlled and estimated to be ~40 nm based on ellipsometry. The thin film morphology was investigated using an atomic force microscope and a scanning electron microscope (SEM). The resultant as-spun films did not exhibit a regular microstructure, but Figure 6a shows the coexistence of disordered structures of lines and of dots. The line structures are derived from the cylindrical PEO microdomains that were oriented parallel to the substrate. The dot structures are most likely the spherical PEO microdomains. Thermal annealing for the as-spun film was performed at 90 °C for 60 s. In Figure 6b, only dot structures of the PEO domains within the PMAPOSS matrix were observed in the film, where the dots formed hexagonal lattices in the polycrystalline structure. Next, to transform the nanostructure of the films, solvent annealing was performed with chloroform vapor for 120 s. As shown in Figure 6c, line nanostructures were formed. A second thermal annealing process at 90 °C for 60 s transformed the nanostructures from lines to dots again (Figure 6d).

The observed morphological changes can be explained by a change in the relative volume fraction of the constituent blocks of the BCP at each annealing state. For the as-spun film, rapid evaporation of the casting solvent, chloroform, during the spin casting did not allow sufficient mobility of the polymer chains of PEO_{143}-*b*-$PMAPOSS_{12}$, leading to the microphase separation to form well-ordered nanostructures in thermodynamic equilibrium. Thermal annealing at

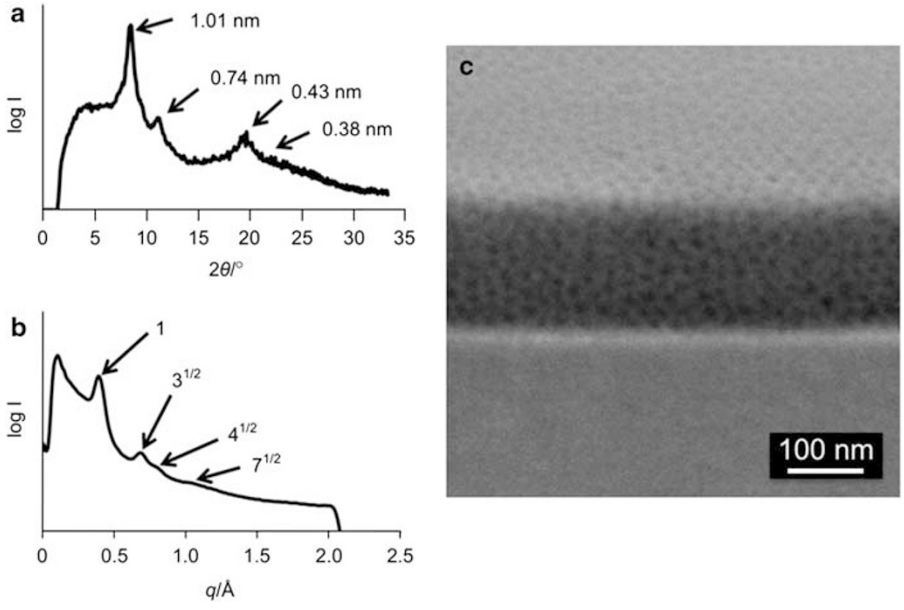

Figure 5 Wide angle X-ray diffraction (WAXD) and SAXS profiles and an SEM image of PEO_{143}-*b*-$PMAPOSS_{12}$. (**a**) WAXD profile, (**b**) SAXS profile and (**c**) SEM image.

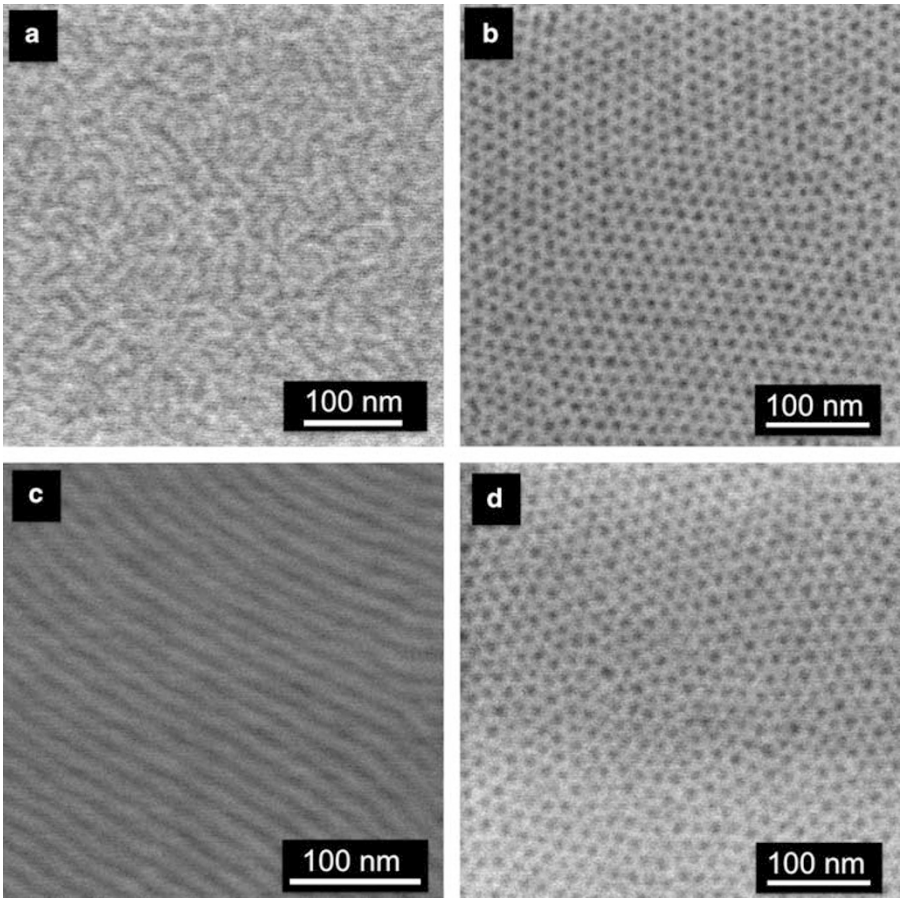

Figure 6 SEM images of PEO_{143}-*b*-$PMAPOSS_{12}$ thin films. (**a**) As-spun cast film, (**b**) thermally annealed film at 90 °C for 60 s, (**c**) solvent annealed film with chloroform vapor for 120 s, (**d**) additional thermal annealing of the film shown in (**c**) at 90 °C for 60 s.

90 °C, which is above the T_m of the PEO block ($T_m = 50$ °C) and the T_g of the PMAPOSS block ($T_g = 82$ °C), induced the formation of hexagonally packed dot nanostructures. As a result of thermal annealing, the volume fraction of the corresponding PEO microdomains in the as-spun film may decrease with the removal of the remaining solvent and with reassembly of the polymer chains in the metastable structures, which possess a relatively larger free volume. In the melt state, the isotropic PEO chains have a significant role for the polymer reassembly. In our previous study of POSS-containing BCPs, neither PS-*b*-PMAPOSS nor PMMA-*b*-PMAPOSS exhibited morphological reassembly following thermal annealing. This may have occurred because the appropriate annealing temperatures exceeded the thermal degradation temperature of the BCPs. Thus, the BCPs are in the amorphous state at these annealing temperatures, and the mobility of the polymer chains is insufficient for reassembly in such a short time. Conversely, with solvent annealing, the chloroform vapor dissolves in the PEO_{143}-*b*-$PMAPOSS_{12}$ and acts as a plasticizer. Because the BCP comprises two immiscible chains, the solvent molecule of chloroform demonstrates different affinities in each microdomain. To investigate the relative solubility of the PEO and PMAPOSS block chains with chloroform, we evaluated the swelling behaviors of the homopolymers of PEO and PMAPOSS. Each silicon-mounted thin film for PEO and PMAPOSS homopolymers was exposed to chloroform vapor, and the degree of swelling was measured *in situ* with the annealing time by measuring the film thickness (Figure 7). Under solvent annealing conditions, almost no change in the degree of swelling was observed until 40 s for both of PEO and PMAPOSS films. After 45 s, abrupt swelling in the PEO film was observed, whereas slight swelling occurred in the PMAPOSS. The degree of swelling for the PEO film in chloroform vapor was ~180% at 55 s. After 120 s, the thickness of PEO film increased from 202 nm up to 522 nm (a 258% increase in thickness). In contrast, the degree of swelling in the PMAPOSS film was 134% for the same annealing duration. These results suggest that chloroform has a selective affinity

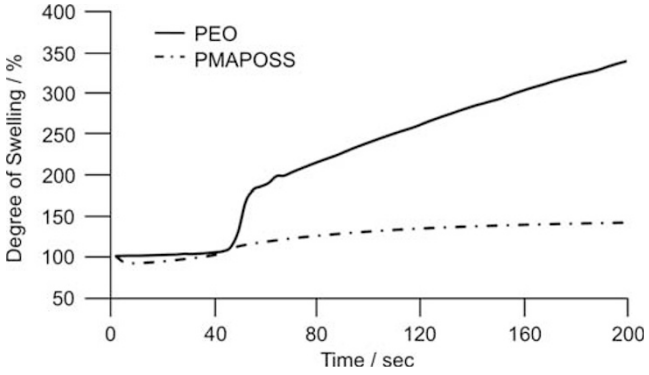

Figure 7 Degree of swelling of PEO homopolymer (solid line) and PMAPOSS homopolymer (dashed line) under saturated chloroform vapor condition.

for PEO. Thus, preferential partitioning of chloroform into the PEO domains is expected in the solvent annealing of the PEO_{143}-*b*-$PMAPOSS_{12}$ thin films. We propose that solvent annealing induces a change in the effective volume fractions of the two constituent blocks and can change the microdomain morphology from spheres to cylinders in this case. The resultant cylinders in the film changed to spherical microdomains again by thermal annealing for 90 s. No change was observed in the size of the dots (12 nm in diameter) before and after this annealing cycle. The center-to-center distances between the dots changed slightly, from 18 to 20 nm. The thicknesses of the films with microdomains of dots, lines and reformed dots were 45 nm, 46 nm and 45 nm, respectively. These results indicate that the PEO_{143}-*b*-$PMAPOSS_{12}$ chains gain the mobility to diffuse and undergo microphase separation to form the self-assembled nanostructure in thermodynamic equilibrium at appropriate annealed stages. The remarkable rapid morphology change in several tens of seconds in this study might be caused by the high mobility of the PEO_{143}-*b*-$PMAPOSS_{12}$ chains in the melt state and swollen state, and by the unique abrupt swelling behavior of PEO at the early stages of solvent annealing.

Rapid formation of hexagonally packed array of dots on a trench-patterned substrate by environment-controlled spin casting

In the previous section, we demonstrated reversible control of the phase morphologies in PEO_{143}-*b*-$PMAPOSS_{12}$ thin films by thermal annealing and solvent annealing. We found that the morphology change occurs rapidly and can be controlled by both of thermal and solvent annealing. On the basis of the remarkably rapid reassembly of PEO_{143}-*b*-$PMAPOSS_{12}$, we attempted to create well-ordered nanostructures in the thin films by spin casting alone, without further annealing.[38,39] We focused on the rapid swelling behavior of PEO with chloroform vapor. Because PEO is easily swollen by chloroform vapor in <60 s, we prepared the PEO_{143}-*b*-$PMAPOSS_{12}$ thin films by spin casting and immediately solvent annealing with chloroform vapor in the spin-coat chamber. First, the PEO_{143}-*b*-$PMAPOSS_{12}$ solution in chloroform was dropped onto a silicon wafer and the wafer was rotated at 4000 r.p.m. for 90 s after closing the lid. Before starting the rotation, a small amount of chloroform ($\sim$30 ml) was sprinkled onto the rotating pedestal. Figure 8a shows the atomic force microscope phase image of the spin-cast PEO_{143}-*b*-$PMAPOSS_{12}$ thin film under this condition. The as-spun film exhibited only a periodic dot nanostructure, which was composed of spherical domains of PEO within the PMAPOSS matrix. In the previous section, the thin film that was annealed with chloroform vapor showed line nanostructures. In this solvent vapor condition, the slight swelling did not induce a change in the volume fraction that could promote the formation of the PEO cylinders, but the swollen PEO_{143}-*b*-$PMAPOSS_{12}$ chains were able to gain enough mobility to diffuse and undergo microphase separation to form dot nanostructures. The small amount of chloroform vapor placed in the chamber may have prevented rapid evaporation during the film formation. The evaporation time was sufficient for the formation of a regular dot nanostructure by microphase separation. Next, we attempted to perform direct self-assembly by graphoepitaxy to prepare the PEO_{143}-*b*-$PMAPOSS_{12}$ thin film. Graphoepitaxy has been demonstrated as an effective strategy to improve the long-range order of microdomains.[40,41] A trench-patterned silicon wafer was used with a groove that was 50 nm deep and 500 nm wide. As shown in Figure 8b, the well-defined hexagonally packed dot pattern in the PEO_{143}-*b*-$PMAPOSS_{12}$ nanostructure was obtained under the same condition. Without any further annealing, PEO_{143}-*b*-$PMAPOSS_{12}$ formed such a regular nanostructure of dots in the thin film using spin casting alone. The fast Fourier-transformed data in Figure 8 (inset images) indicated that a trench-patterned silicon wafer effectively aligned the dot patterns in the PEO_{143}-*b*-$PMAPOSS_{12}$ nanostructure.

CONCLUSION

In summary, we have demonstrated that the combination of thermal annealing and solvent annealing can produce a reversible, rapid nanostructure change between dots and lines in PEO_{143}-*b*-$PMAPOSS_{12}$ thin films. The PEO_{143}-*b*-$PMAPOSS_{12}$ polymer was successfully synthesized by atom transfer radical polymerization of POSS methacrylate in the presence of a PEO macroinitiator. The disordered, coexisting line and dot nanostructure in the as-spun film changed to a hexagonally packed dot nanostructure of the PEO spherical domains, after thermal annealing at 90 °C for 60 s. Solvent annealing the film with chloroform vapor for 120 s led to the reassembly of the polymer chains to form line nanostructures. The line structures were transformed back to dot structures by thermal annealing under the previously used conditions. Both thermal and solvent annealing for short durations provided sufficient mobility of the PEO_{143}-*b*-$PMAPOSS_{12}$ chains to form the self-assembled nanostructures in thermodynamic equilibrium. We also successfully prepared PEO_{143}-*b*-$PMAPOSS_{12}$ thin films with hexagonally packed dot arrays by spin

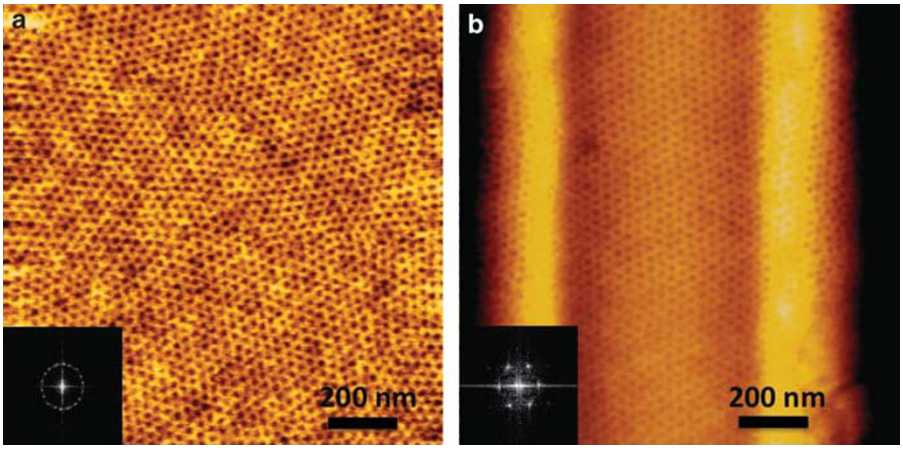

Figure 8 Atomic force microscope phase images of PEO_{143}-*b*-$PMAPOSS_{12}$ thin films prepared by spin casting under chloroform vapor for 90 s. (**a**) on a flat Si substrate, (**b**) on a trench-patterned Si substrate with a groove that was 50 nm deep and 500 nm wide.

casting onto a trench-patterned silicon substrate under chloroform vapor conditions without any additional annealing. The key factor for the successful, rapid formation and change in nanostructure was the mobility of the PEO chains in the BCP of PEO_{143}-*b*-$PMAPOSS_{12}$. The PEO chains, with high mobility in the BCP, had a significant role in the self-assembly and reassembly of the nanostructure. The ability to reversibly tune the phase morphology in BCP thin films can be applied to create a variety of patterned nanotemplates.

ACKNOWLEDGEMENTS

We gratefully thank Mr Ryohei Kikuchi, of the Center for Ascended Materials Analysis at the National University Corporation Tokyo Institute of Technology, for TEM measurement.

1 Lazzari, M. & Lopez-Quintela, M. A. Block copolymers as a tool for nanomaterial fabrication. *Adv. Mater.* **15,** 1583–1594 (2003).
2 Park., C., Yonn, J. & Thomas, E. L. Enabling nanotechnology with self assembled block copolymer patterns. *Polymer* **44,** 6725–6760 (2003).
3 Ruzette, A. V. & Leibler, L. Block copolymers in tomorrow's plastics. *Nat. Mater.* **4,** 19–31 (2005).
4 Halmley, IW. *The Physics of Block Copolymers* (Oxford University Press, Oxford, 1998).
5 Fasolka, M. & Mayes, A. M. Block copolymer thin films: physics and applications. *Annu. Rev. Mater. Res.* **31,** 323–355 (2001).
6 Kim, H.-C., Park, S.-M. & Hinsberg, W. D. Block copolymer based nanostructures: materials, processes, and applications to electronics. *Chem. Rev.* **110,** 146–177 (2010).
7 Galatsis, K., Wang, K. L., Ozkan, M., Ozkan, C. S., Huang, Y., Chang, J. P., Monbouquette, H. G., Chen, Y., Nealey, P. & Botros, Y. Patterning and templating for nanoelectronics. *Adv. Mater.* **22,** 769–778 (2010).
8 Cheng, J. Y., Ross, C. A., Smith, H. I. & Thomas, E. L. Templated self-assembly of block copolymers: top-down helps bottom-up. *Adv. Mater.* **18,** 2505–2521 (2006).
9 Park, M, Harison, C., Chaikin, P. M., Register, R. A. & Adamson, D. H. Block copolymer lithography: periodic arrays of $\sim 10^{11}$ holes in 1 square centimeter. *Science* **276,** 1401–1404 (1997).
10 Hawker, C. J. & Russell, T. P. Block copolymer lithography: merging 'Bottm-Up' with 'Top-Down' processes. *MRS Bull.* **30,** 952–966 (2005).
11 Bang, J., Jeong, U., Ryu, D. Y., Russell, T. P. & Hawker, C. J. Block copolymer nanolithography: translation of molecular level control to nanoscale patterns. *Adv. Mater.* **21,** 4769–4792 (2009).
12 Ruiz, R., Kang, H., Detcheverry, F. A., Dobisz, E., Kercher, D. S., Albrecht, T. R., de Pablo, J. J. & Nealey, P. F. Density multiplication and improved lithography by directed block copolymer assembly. *Science* **321,** 936–939 (2008).
13 Kim, S. O., Solak, H. H., Stoykovich, M. P., Ferrier, N. J., de Pablo, J. J. & Nealey, P. F. Epitaxial self-assembly of block copolymers on lithographically defined nanopatterned substrates. *Nature* **424,** 411–414 (2003).
14 Black, C. T., Guarini, K. W., Milkove, K. R., Baker, S. M. & Russell, T. P. Integration of self-assembled diblock copolymers for semiconductor capacitor fabrication. *Appl. Phys. Lett.* **79,** 409–411 (2001).
15 Kim, H.-C. & Russell, T. P. Ordering in thin films of asymmetric diblock copolymers. *J. Polym. Sci.: Part B: Polym. Phys.* **39,** 663–668 (2001).
16 Jung, Y. S. & Ross, C. A. Orientation-controlled self-assembled nanolithography using a polystyrene-polydimethylsiloxane block copolymer. *Nano. Lett.* **7,** 2046–2050 (2007).
17 Bita, I., Yang, J. K. W., Jung, Y. S., Ross, C. A., Thomas, E. L. & Berggren, K. K. Graphoepitaxy of self-assembled block copolymers on two-dimensional periodic patterned templates. *Science* **321,** 939–943 (2008).
18 Xiao, S., Yang, X. M., Park, S., Weller, D. & Russell, T. P. A Novel approach to addressable 4 teradot/in.^{2} Patterned media. *Adv. Mater.* **21,** 2516–2519 (2009).
19 Rider, D. A., Liu, K., Eloi, J.-C., Vanderark, L., Yang, L., Wang, J.-Y., Grozea, D., Lu, Z.-H., Russell, T. P. & Manners, I. Nanostructured magnetic thin films from organometallic block copolymers: pyrolysis of self-assembled polystyrene-block- poly (ferrocenylethylmethylsilane). *ACS Nano* **2,** 263–270 (2008).
20 Cheng., J. Y., Zhang, F., Smith, H. I., Vancso, G. J. & Ross, C. A. Pattern registration between spherical block-copolymer domains and topographical templates. *Adv. Mater.* **18,** 597–601 (2006).
21 Rider, D. A., Cavicchi, K. A., Vanderark, L., Russell, T. P. & Manners, I. Orientationally controlled nanoporous cylindrical domains in polystyrene-*b*-poly(ferrocenylethyll-methylsilane) block copolymer films. *Macromolecules* **40,** 3790–3796 (2007).
22 Hirai, T., Leolukman, M., Hayakawa, T., Kakimoto, M. & Gopalan, P. Hierarchical nanostructures of organosilicate nanosheets within self-organized block copolymer films. *Macromolecules* **41,** 4558–4560 (2008).
23 Hirai, T., Leolukman, M., Liu, C. C., Han, E., Kim, Y. J., Ishida, Y., Hayakawa, T., Kakimoto, M., Nealey, P. F. & Gopalan, P. One-step direct-patterning template utilizing self-assembly of POSS-containing block copolymers. *Adv. Mater.* **21,** 4334–4338 (2009).
24 Hirai, T., Leolukman, M., Jin, S., Goseki, R., Ishida, Y., Kakimoto, M., Hayakawa, T., Ree, M. & Gopalan, P. Hierarchical self-assembled structures from POSS-containing block copolymers synthesized by living anionic polymerization. *Macromolecules* **42,** 8835–8843 (2009).
25 Ishida, Y., Tada, Y., Hirai, T., Goseki, R., Kakimoto, M., Yoshida, H. & Hayakawa, T. Directed self-assembly of cage silsesquioxane containing block copolymers via graphoepitaxy techniques. *J. Photopolym. Sci. Technol.* **23,** 155–159 (2010).
26 Ishida, Y., Hirai, T., Goseki, R., Tokita, M., Kakimoto, M. & Hayakawa, T. Synthesis and self-assembly of thermotropic block copolymer with long alkyl tethered cage silsesquiovane in the side chain. *J. Poly. Sci. A, Polym. Chem.* **49,** 2653–2664 (2011).
27 Tada, Y., Yoshida, H., Ishida, Y., Hirai, T., Bosworth, J. K., Dobisz, E., Ruiz, R., Takenaka, M., Hayakawa, T. & Hasegawa, H. Directed self-assembly of POSS containing block copolymer on lithographically defined chemical template with morphology control by solvent vapor. *Macromolecules* **45,** 292–304 (2012).
28 Bosworth, J. K., Black, C. T. & Ober, C. K. Selective area control of self-assembled pattern architecture using a lithographically patternable block copolymer. *ACS Nano* **3,** 1761–1766 (2009).
29 Paik, M. Y., Bosworth, J. K., Smilgies, D.-M., Schwartz, E. L., Andre, X. & Ober, C. K. Reversibly morphology control in block copolymer films via solvent vapor processing: an in situ GISAXS Study. *Macromolecules* **43,** 4253–4260 (2010).
30 Krausch, G. & Magerle, R. Nanostructured thin films via self-assembly of block copolymers. *Adv. Mater.* **14,** 1579–1583 (2002).
31 Zhao, J., Jiang, S., Ji, X., An, L. & Jiang, B. Study of the time evolution of the surface morphology of thin asymmetric diblock copolymer films under solvent vapor. *Polymer* **46,** 6513–6521 (2005).
32 Kim, G. & Libera, M. Morphological development in solvent-cast polystyrene-polybutadiene-polystyrene (SBS) triblock copolymer thin films. *Macromolecules* **31,** 2569–2577 (1998).
33 Welander, A. M., Kang, H., Stuen, K. O., Solak, H. H., Mueller, M., de Pablo, J. J. & Nealey, P. F. Rapid directed assembly of block copolymer films at elevated temperatures. *Macromolecules* **41,** 2759–2761 (2008).
34 Hussain, H., Tan, B. H., Seah, G. L., Lin, Y., He, C. B. & Daris, T. P. Micelle formation and gelation of (PEG-P(MA-POSS)) amphiphilic block copolymers via associative hydrophobic effects. *Langmuir* **26,** 11763–11773 (2010).
35 Tan, B. H., Hussain, H. & He, C. B. Tailoring micelle formation and gelation in (PEG-P(MA-POSS)) amphiphilic hybrid block copolymers. *Macromolecules* **44,** 622–631 (2011).
36 Mya, K. Y., Lin, E. M. J., Gudipati, C. S., Shen, L. & He, C. Time-dependent polymerization kinetic study and the properties of hybrid polymers with functional silsesquioxanes. *J. Phys. Chem. B* **114,** 9119–9127 (2010).
37 Pyun, J., Matyjaszewski, K., Wu, J., Kim, G.-M., Chun, S. B. & Mather, P. T. ABA triblock copolymers containing polyhedral oligomeric silsesquioxane pendant groups: synthesis and unique properties. *Polymer* **44,** 2739–2750 (2003).
38 Kim, S., Briber, R. M., Karim, A., Jones, R. L. & Kim, H.-C. Environment-controlled spin coating to rapidly orient microdomains in thin block copolymer films. *Macromolecules* **40,** 4102–4105 (2007).
39 Kim, S. H., Minster, M. J., Xu, T., Kimura, M. & Russell, T. P. Highly oriented and ordered arrays from block copolymers via solvent evaporation. *Adv. Mater.* **16,** 226–231 (2004).
40 Segalman, R. A., Yokoyama, H. & Kramer, E. J. Graphoepitaxy of spherical domain block copolymer films. *Adv. Mater.* **13,** 1152–1155 (2001).
41 Yamaguchi, T. & Yamaguchi, H. Two-dimensional patterning of flexible designs with high half-pitch resolution by using block copolymer lithography. *Adv. Mater.* **20,** 1684–1689 (2008).